High energy density PbO2/activated carbon asymmetric electrochemical capacitor based on lead dioxide electrode with three-dimensional porous titanium substrate

ARTICLE *in* INTERNATIONAL JOURNAL OF HYDROGEN ENERGY · SEPTEMBER 2014

Impact Factor: 3.31 · DOI: 10.1016/j.ijhydene.2014.08.039

INTERNATIONAL JOURNAL OF HYDROGEN ENERGY 39 (2014) 17153–17161

Available online at www.sciencedirect.com

ScienceDirect

journal homepage: www.elsevier.com/locate/he

High energy density PbO_2/activated carbon asymmetric electrochemical capacitor based on lead dioxide electrode with three-dimensional porous titanium substrate

Wenli Zhang [a], *Haibo Lin* [a,b,*], *Haishen Kong* [a], *Haiyan Lu* [a,*], *Zhe Yang* [a], *Tingting Liu* [a]

[a] *College of Chemistry, Jilin University, Changchun 130012, China*
[b] *Key Laboratory of Physics and Technology for Advanced Batteries of Ministry of Education, Jilin University, Changchun 130012, China*

ARTICLE INFO

Article history:
Received 20 June 2014
Received in revised form
28 July 2014
Accepted 2 August 2014
Available online 4 September 2014

Keywords:
Lead dioxide electrode
Porous titanium substrate
Electrodeposition
Asymmetric electrochemical capacitor
High energy density

ABSTRACT

A PbO_2/AC asymmetric electrochemical capacitor (AEC) with energy density as high as 49.4 Wh kg^{-1}, power density of 433.2 W kg^{-1} and specific capacitance of 135.2 F g^{-1} was fabricated with PbO_2 electrodeposited on three-dimensional porous titanium (3D-Ti/PbO_2) and activated carbon. The high electrochemical active surface of 3D-Ti/PbO_2 resulted in high specific capacity making it suitable for use as positive electrode in PbO_2/AC AEC. The fabricated AEC demonstrated good power performance with an energy density conservation of 30 Wh kg^{-1} at power density of 2078 W kg^{-1}. The fabricated AEC also showed excellent cycling stability with capacitance retention of 99.2% after 1000 cycles.

Introduction

To reduce the emission of carbon dioxide and contaminants, great attention has been paid on renewable power sources such as wind and photovoltaic energy. For the fortuitous and intermittent characteristics of renewable energy, the prerequisite of utilizing renewable energy is reliable energy conversion and storage device [1]. Lead acid battery is a safe and cost effective energy storage device in renewable energy storage [2–6]. Nevertheless, lead acid battery works under partial state of charge in renewable energy storage, which leads to the irreversible sulfation of negative electrode and shortened lifespan [7].

Recently, electrochemical capacitor has interested researchers worldwide, owing to its high power performance and long lifespan [8–10]. PbO_2/AC asymmetric electrochemical capacitor (AEC) is a novel electrochemical capacitor

* *Corresponding authors*. College of Chemistry, Jilin University, Changchun 130012, China. Tel./fax: +86 431 85155189.
E-mail addresses: lhb910@jlu.edu.cn, lhb1963@yeah.net, lhb910@yahoo.com (H. Lin), luhy@jlu.edu.cn (H. Lu).
http://dx.doi.org/10.1016/j.ijhydene.2014.08.039

based on lead acid battery technology [11–13]. Since the PbO_2/AC AEC replaces the negative electrode of Pb in lead acid battery with AC, the sulfation of negative electrode is completely avoided. As a result, the PbO_2/AC AEC has a much longer lifespan than lead acid battery. Hence, the PbO_2/AC AEC is a potential candidate for renewable energy storage owing to its long-lifespan feature.

The positive and negative electrodes of PbO_2/AC AEC store energy via different mechanisms. AC stores energy via electrical double layer, which is a fast process; while PbO_2 stores energy via faradaic reaction, which is a slow process. In order to match the power performance of PbO_2 with that of AC, PbO_2 electrode should have the ability to charge and discharge at high current densities. The pasted PbO_2 electrode has been used in lead acid battery industry over one hundred years [14]. However, pasted PbO_2 electrode fails prematurely due to softening of active material, especially when it is discharged at high current densities [15,16]. Therefore, the pasted PbO_2 electrode can't satisfy the power requirements of PbO_2/AC AEC. By contrast, the PbO_2 electrode with planar titanium substrate (Ti/PbO_2) prepared by electrodeposition possesses good continuity of active material, high stability and good power performance, and it is usually used as the positive electrode in PbO_2/AC AEC [12,13], Nevertheless, Ti/PbO_2 has low capacity and the PbO_2/AC AEC based on Ti/PbO_2 has relatively low energy density [12], which restricts its application in renewable energy storage. Therefore, the preparation of Ti/PbO_2 with high capacity is of great significance.

The energy storage ability of PbO_2 electrode has been widely investigated [17–24]. In summary, the PbO_2 electrode with high capacity and good stability should satisfy the following two conditions: (i) large electrochemical active surface area; (ii) good physical continuity of active material. In order to enhance the surface area and capacity of the planar Ti/PbO_2, Perret and Bartlett [25–27] have prepared nanowire-PbO_2 electrode via template method. The nanowire-PbO_2 electrode possesses higher surface area and capacity than traditional Ti/PbO_2. However, template method is complicated and expensive. A simple and facile method to prepare PbO_2 with large surface area is using substrate with large surface area, such as carbon foam [28]. Nevertheless, carbon foam and other carbon materials experience oxidation at high potentials in concentrated sulfuric acid [29]. Three-dimensional (3D) porous titanium is of good conductivity with both high surface area and anti-corrosion characteristic, which can be used as electrode substrate [30]. In this paper, a PbO_2 electrode with high capacity was electrodeposited with 3D porous titanium as substrate (3D-Ti/PbO_2). Furthermore, A PbO_2/AC AEC based on 3D-Ti/PbO_2 was fabricated with commercial AC as corresponding negative electrode. The PbO_2/AC AEC based on 3D-Ti/PbO_2 demonstrated high specific capacitance, high energy density and long lifespan.

Experimental

Preparation of 3D-Ti/PbO_2

Firstly, planar titanium plates and 3D porous titanium plates with average pore diameter of 60 μm (TA1, Baoji Titanium Industry Co., Ltd.) were polished with emery paper and degreased with 10 wt% NaOH. Secondly, the titanium plates were etched in an aqueous solution of 30 wt% HCl at 100 °C for 1 h, and then the titanium plates were rinsed and reserved in deionized water. Finally, a SnO_2–Sb_2O_5 intermediate layer was prepared on the titanium plates by thermal decomposition as described in reference [31]. The purpose of the preparation of SnO_2–Sb_2O_5 intermediate layer is to increase the conductivity of electrodes and prevent the formation of TiO_2 both in the electrodeposition process and in the charge–discharge process of PbO_2 electrode.

Ti/PbO_2 and 3D-Ti/PbO_2 were prepared on a potentiostat–galvanostat (HYL-A, Yanbian Yongheng Co., China) by anodic electrodeposition in a conventional electrolytic cell with one compartment. The titanium plates with SnO_2–Sb_2O_5 intermediate layer (1.0 × 1.0 cm^2) were used as anodes. A Ti mesh (2.5 × 2.5 cm^2) was used as cathode. The electrolyte was 100 mL solution of 0.5 mol L^{-1} $Pb(NO_3)_2$ and 1.0 mol L^{-1} HNO_3. The deposition current and charge quantity were 1.0 mA cm^{-2} and 9.0 C cm^{-2}, respectively. Analytical reagents and deionized water (resistivity of 18.25 MΩ cm) were used in all experiments.

Preparation of AC electrode and fabrication of 3D-Ti/PbO_2/AC AEC

Activated carbon (AC) (YP-50F, Kuraray, Japan) with a specific surface area of 1600 m^2 g^{-1} was used to prepare the negative electrodes of 3D-Ti/PbO_2/AC AEC. The negative active materials were prepared by mixing AC (85 wt%), acetylene black (10 wt%) and PTFE (5 wt%) to form a mixture with ethanol soaking. The mixture was rolled into a film (1 × 1 cm^2) and attached to stainless steel mesh to form AC electrode. Subsequently, AC electrode was dried in a vacuum oven at 100 °C overnight to evaporate ethanol. The 3D-Ti/PbO_2/AC AEC was fabricated using 3D-Ti/PbO_2 as positive electrode and AC as negative electrode with a polypropylene diaphragm in the middle. An aqueous solution of 1.0 mol L^{-1} H_2SO_4 was used as the electrolyte in the 3D-Ti/PbO_2/AC AEC.

Physical and electrochemical characterization

The microstructure of the PbO_2 was detected with X-ray diffraction (XRD) on a D/max diffractometer (Ragaku, Japan) with Cu-Kα radiation source (λ = 1.541874 Å) operating at 50.0 kV and 200.0 mA. A SU8020 scanning electron microscope (SEM) (HITACHI, Japan) was employed to characterize the surface morphology of PbO_2 electrodes. The electrochemical performances of single electrode and 3D-Ti/PbO_2/AC AEC were tested on PARSTAT 2273 electrochemical work station (Princeton Applied Research, USA) in a conventional three-electrode cell. In three-electrode system, a Ti/RuO_2–TiO_2 electrode was used as the counter electrode, a KCl-saturated calomel electrode (SCE) was used as the reference electrode and all the potentials were quoted with respect to SCE. The impedance characteristics of 3D-Ti/PbO_2/AC AEC was tested by alternating current electrochemical impedance spectroscopy (EIS) at 1.8 V in the frequency range of 100 kHz–100 mHz with a voltage amplitude of 10 mV. The galvanostatic

charge–discharge test of 3D-Ti/PbO_2/AC AEC was performed on a BTS battery test system (Neware, China).

Results and discussion

Characterization of 3D-Ti/PbO_2

Structure and morphology of 3D-Ti/PbO_2

XRD patterns of 3D-Ti/PbO_2 and Ti/PbO_2 are presented in Fig. 1. The PbO_2 on both electrodes were mixture phases of β-PbO_2 (JCPDS card No. 14-4192) and α-PbO_2 (JCPDS card No. 37-0517). The diffractive peak at 36.2° corresponds to the (020) crystal plane of β-PbO_2, where Ti/PbO_2 had high intensity indicating the preferential growth of PbO_2 on Ti/PbO_2. The XRD pattern of 3D-Ti/PbO_2 had no strong peaks at any crystal planes indicating the non-preferential growth of PbO_2. The non-preferential growth of PbO_2 is favorable to enriching crystal orientation and enlarging electrochemical active surface area.

In order to compare the influence caused by different substrates, the deposition charge quantity and current density were precisely controlled at 9.0 C cm^{-2} and 1 mA cm^{-2}, respectively. The current efficiency and the mass of active material of Ti/PbO_2 and 3D-Ti/PbO_2 were both 99.6% and 11.1 mg. The SEM images of planar titanium, 3D porous titanium, Ti/PbO_2 and 3D-Ti/PbO_2 are shown in Fig. 2. Fig. 2a shows the SEM image of planar substrate with explanate surface. Fig. 2b shows the SEM image of 3D porous titanium substrate. As can be seen, 3D porous titanium substrate had irregular pores with average diameter of about 60 μm. Hence, the 3D porous titanium substrate can provide larger surface area than the planar substrate in electrodeposition process. Fig. 2c and d shows the SEM images of Ti/PbO_2 and 3D-Ti/PbO_2, respectively. The size of the PbO_2 particle at Ti/PbO_2 was as large as 6 μm, while 3D-Ti/PbO_2 had numbers of nanoparticles with average diameter of 300 nm. The very small PbO_2 nanoparticles could provide large active surface for 3D-Ti/PbO_2. The origin of small nanoparticles results from the small real current density at 3D porous titanium substrate [32,33], since the 3D porous titanium substrate has a much larger surface area than planar titanium substrate. Under a large current density on planar substrate, the nucleation is preferential and numerous nucleis crash together forming large particle. While on the 3D porous titanium substrate, the real current density is much smaller and both the nucleation and growth are not preferential, small particles are formed.

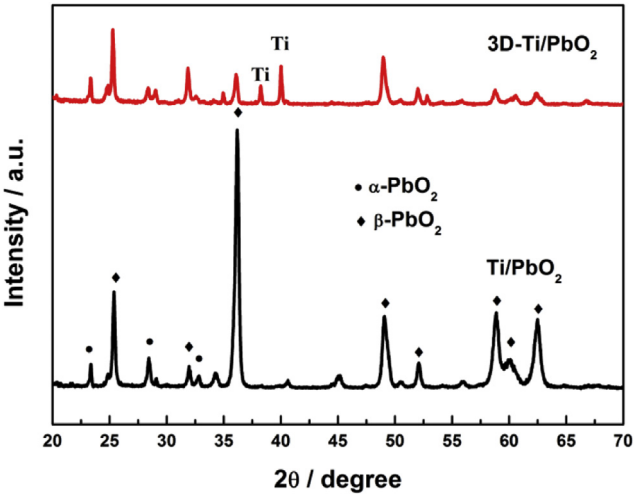

Fig. 1 – XRD patterns of Ti/PbO_2 and 3D-Ti/PbO_2.

Electrochemical characterization of 3D-Ti/PbO_2

The cyclic voltammograms of 3D-Ti/PbO_2 and Ti/PbO_2 are presented in Fig. 3a. The cathodic peak at 1.25 V is attributed to the reduction of PbO_2, and the anodic peak at 1.8 V is attributed to the oxidation of $PbSO_4$ (Eq. (1)).

$$PbSO_4 + 2H_2O \leftrightarrow PbO_2 + HSO_4^- + 3H^+ + 2e^- \quad (1)$$

The charge quantity of the transformation between $PbSO_4$ and PbO_2 of 3D-Ti/PbO_2 was almost four times as large as that of Ti/PbO_2. It means that 3D-Ti/PbO_2 has a much higher capacity than Ti/PbO_2.

Fig. 3b shows the galvanostatic charge–discharge curves of 3D-Ti/PbO_2 and Ti/PbO_2. Both discharge curves showed the "plateau" at potential of 1.3 V. Ti/PbO_2 had a small capacity of 20.8 mAh g^{-1}. This results from the reason that Ti/PbO_2 has small surface area and continuous $PbSO_4$ film formed in the initial discharge process. The continuous $PbSO_4$ film is neither favorable to the reactant transportation nor favorable to the electron conduction in discharge. By contrast, 3D-Ti/PbO_2 had a much higher capacity (132 mAh g^{-1}) than Ti/PbO_2. The high specific capacity could results from the large electrochemical active surface area of 3D-Ti/PbO_2. In this paper, voltammetric charge (q*) was used to determine the electrochemical active surface area of PbO_2 electrodes.

The electrochemical active surface area means the active sites accessible to the electrolyte when electrochemical reaction occurs [34]. The q* can quantitatively reflect the electrochemical active surface area [35–37]. The larger is the q*, the larger is the electrochemical active surface area. In sulfate solution, special adsorption occurs on the surface of PbO_2 (Eqs. (2) and (3)), and PbO_2 is electrochemically transformed into insoluble $PbSO_4$ resulting in pseudo-capacitance [38].

$$H^+ + SO_{4ads}^{2-} \leftrightarrow HSO_{4ads}^- \quad (2)$$

$$4HSO_{4ads}^- + PbO_2 + 2e^- \leftrightarrow PbSO_{4ads} + 3SO_{4ads}^{2-} + H_2O \quad (3)$$

Hence, the q* in the pseudo-capacitance region of PbO_2 in sulfate solutions can be defined as the electrochemical active surface area when PbO_2 reacts with electrolyte containing sulfate ion. The H_2SO_4 solution is not applied in this test, because both the surfaces and inner layers of PbO_2 interact with H_2SO_4. The cyclic voltammograms of Ti/PbO_2 and 3D-Ti/PbO_2 in 0.5 mol L^{-1} Na_2SO_4 solution are shown in Fig. 3c and d shows the q* integrated from the cyclic voltammograms. As can be seen, the q* of 3D-Ti/PbO_2 was much larger than the q* of Ti/PbO_2 at all scan rates. At a low scan rate of 10 mV s^{-1}, the q* of 3D-Ti/PbO_2 was 33 mC cm^{-2}, while the q* of Ti/PbO_2 was only 10 mC cm^{-2}. At a high scan rate of 110 mV s^{-1}, the q* of 3D-Ti/PbO_2 was 15 mC cm^{-2} which was five times as large as that of Ti/PbO_2 (3 mC cm^{-2}). The high electrochemical active surface area of 3D-Ti/PbO_2 results from the large surface area

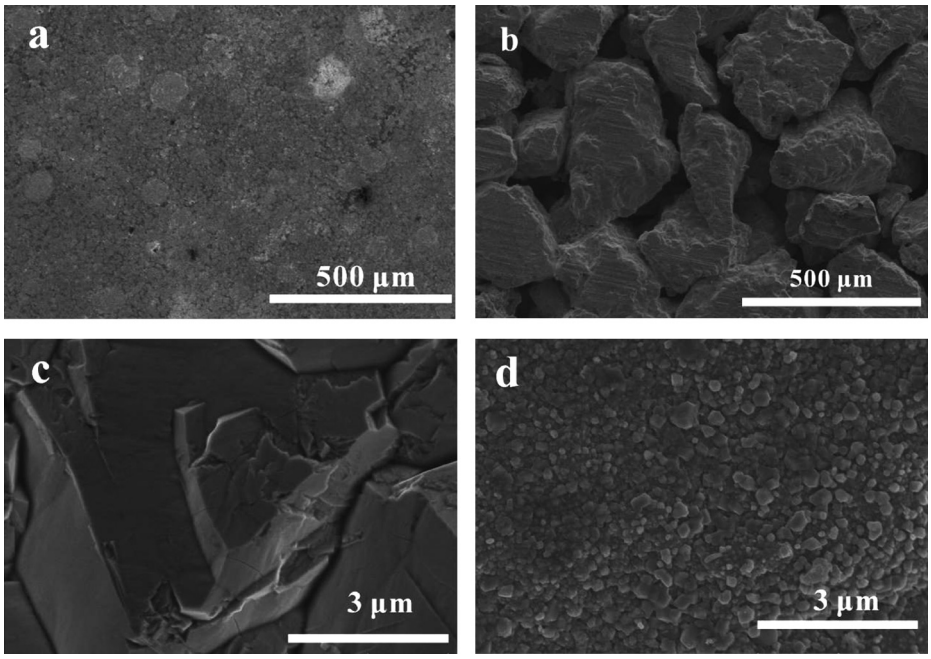

Fig. 2 – SEM images of (a) planar titanium substrate and (b) 3D porous titanium substrate coated with SnO_2–Sb_2O_5 intermediate layer; Surfaces of (b) Ti/PbO_2 and (c) 3D-Ti/PbO_2.

of 3D porous titanium substrate, abundance of crystal orientation of PbO_2 on 3D-Ti/PbO_2 and numerous nanoparticles on the 3D-Ti/PbO_2. In summary, 3D-Ti/PbO_2 has a much larger electrochemical active surface area than Ti/PbO_2, which is the main reason for the high capacity of 3D-Ti/PbO_2.

Performances of 3D-Ti/PbO_2/AC AEC

Fabrication of 3D-Ti/PbO_2/AC AEC

The configuration of an AEC is the combination of positive electrode capacitor and negative electrode capacitor in series.

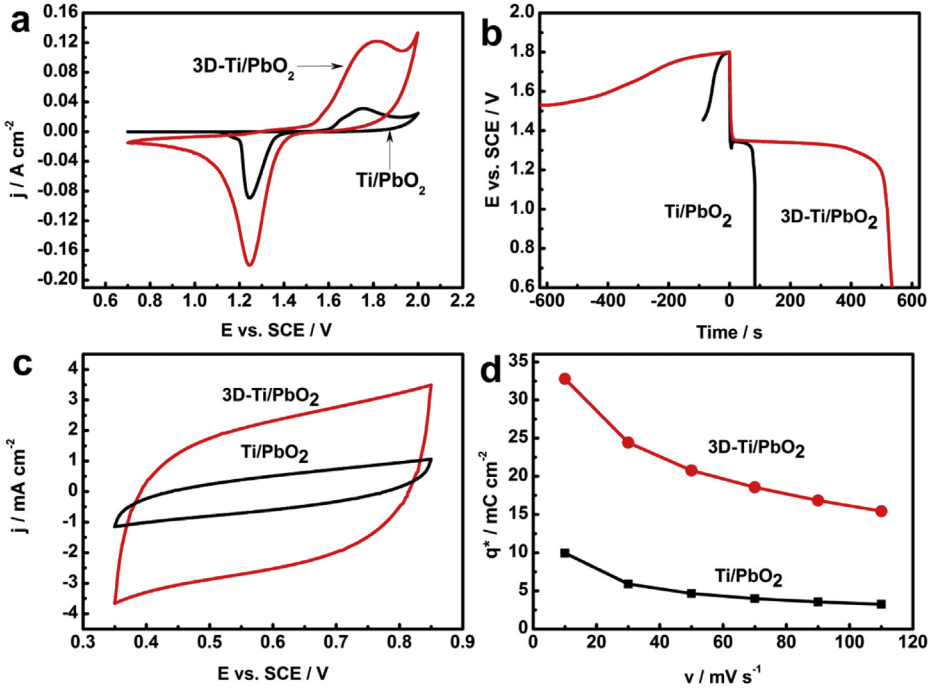

Fig. 3 – (a) Cyclic voltammograms of Ti/PbO_2 and 3D-Ti/PbO_2 in 1.0 mol L^{-1} H_2SO_4 solution at 20 mV s^{-1}; (b) Galvanostatic charge–discharge curves of Ti/PbO_2 and 3D-Ti/PbO_2 in 1.0 mol L^{-1} H_2SO_4 solution at 0.9 A g^{-1}; (c) Cyclic voltammograms of 3D-Ti/PbO_2 and Ti/PbO_2 in 0.5 mol L^{-1} Na_2SO_4 solution at 50 mV s^{-1}; (d) Relationship of voltammetric electric quantity (q*) versus scan rate.

The reciprocal of total capacitance is the summation of the reciprocal of negative capacitance and the reciprocal of positive capacitance (Eq. (4)) [10]:

$$\frac{1}{C_T} = \frac{1}{C_P} + \frac{1}{C_N} \quad (4)$$

In Eq. (4), C_T is the total capacitance of an AEC, C_P is the capacitance of positive electrode, and C_N is the capacitance of negative electrode. For the PbO_2/AC AEC, the higher is the capacity of PbO_2 electrode, the closer the capacitance of AEC goes to the capacitance of AC electrode. Therefore, the high capacity characteristic of 3D-Ti/PbO_2 will greatly improve the capacitive performance of PbO_2/AC AEC.

Cyclic voltammograms of 3D-Ti/PbO_2 and AC electrodes are shown in Fig. 4a. As can be seen, the cyclic voltammogram of AC electrode had a symmetric shape in the potential range of −0.5 V to 0.9 V, indicating the good capacitive performance of AC electrode. The electrochemical behavior of 3D-Ti/PbO_2 is caused by the transformation between PbO_2 and $PbSO_4$.

Fig. 4b shows the galvanostatic charge–discharge curves of 3D-Ti/PbO_2 and AC electrode. The different shapes of 3D-Ti/PbO_2 and AC electrode indicate different energy storage mechanisms. Namely, PbO_2 stores energy via faradaic reaction, while AC stores energy via electric double layer. These two half cells can be assembled to a PbO_2/AC AEC based on 3D-Ti/PbO_2 (3D-Ti/PbO_2/AC). The end voltage of charge and the voltage beginning to discharge were 2.3 V and 1.8 V, respectively. The difference between these two values is mainly attributed to polarization of the PbO_2 electrode. An inflexion point appeared at the end of discharge, indicating the deep discharge of PbO_2 positive electrode. Although the voltage of 0 V can be reached as read from Fig. 4b, the discharge process from the voltage of inflexion point to 0 V delivers a little energy (low surface area between the two discharge curves). For the certain 3D-Ti/PbO_2 in this experiment, the energy stored in the AEC depends on the amount of AC. The larger is the amount of AC, the slower the potential of AC ascends when the AEC is discharged. In the meantime, the larger is the area between these two charge–discharge curves and the more energy the AEC stores. But the energy density is not in the same situation, the energy density may reach the highest value at a certain amount of AC [12].

Cyclic voltammetry was used to investigate the energy storage characteristic of 3D-Ti/PbO_2/AC AEC (Fig. 5a). As can be seen, the charge current was small unless the voltage comes to 1.0 V, while the discharge current became large when the voltage dropped below 1.9 V. The charge current increased sharply when the voltage was close to 2.4 V, which means that the voltage is too high for charge and water in the electrolyte is decomposed. Thus, the concentration of sulfuric acid increases, which will make the PbO_2 electrode passivated [39]. Therefore, the end voltage of charge should be strictly restricted at or below 2.3 V according to Fig. 4b.

Fig. 5b shows the charge–discharge curve of 3D-Ti/PbO_2/AC AEC. The discharge curve can be divided into three parts by two inflexion points at 1.8 V and 0.8 V [12]. The first part of

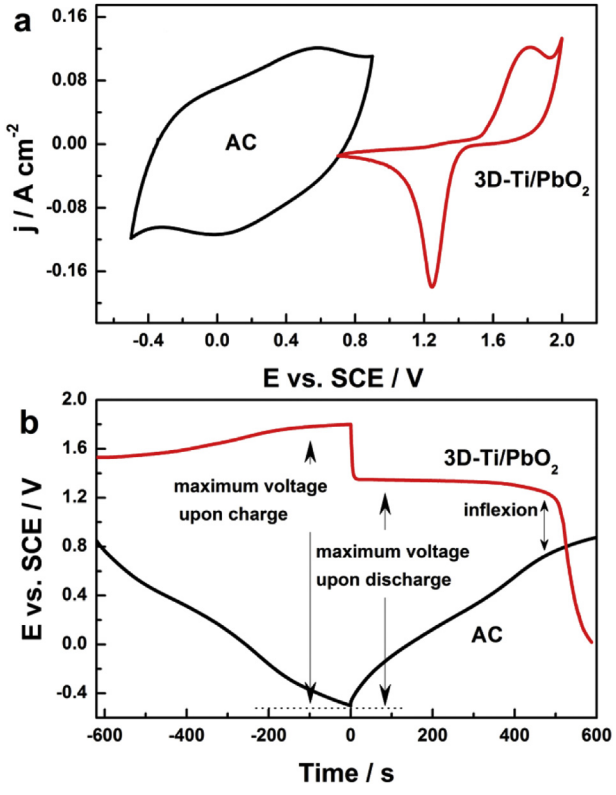

Fig. 4 – (a) Cyclic voltammograms of 3D-Ti/PbO_2 and AC electrode in 1.0 mol L^{-1} H_2SO_4 solution at 20 mV s^{-1}; (b) Galvanostatic charge–discharge curves of individual electrodes of 3D-Ti/PbO_2 and AC in 1.0 mol L^{-1} H_2SO_4 solution at 10 mA cm^{-2}.

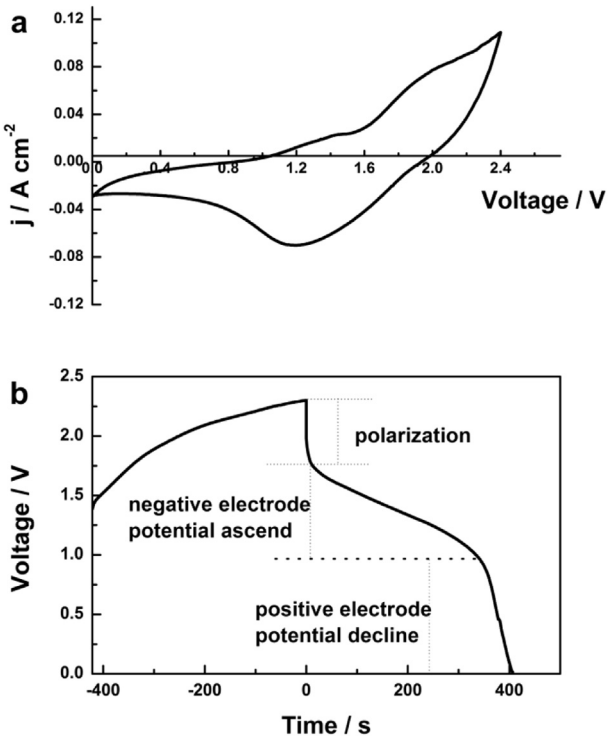

Fig. 5 – (a) Cyclic voltammogram of the 3D-Ti/PbO_2/AC AEC in 1.0 mol L^{-1} H_2SO_4 solution at 20 mV s^{-1}; (b) Galvanostatic charge–discharge curve of 3D-Ti/PbO_2/AC AEC at 10 mA cm^{-2}.

discharge curve declined sharply. It results from the polarization of positive electrode. The second part was an oblique line (0.8 V–1.8 V) where the voltage changed linearly with discharge time. The reason is that during this voltage range the potential of positive electrode comes to a plateau, and the potential of negative electrode changes linearly (Fig. 4b). The potential of the third part of discharge curve decreased sharply due to the deep discharge of positive electrode. There is a little energy delivering from the AEC during the third part of discharge curve. Hence, the capacitive behavior of 3D-Ti/PbO_2/AC AEC is mainly related to the second part of the discharge curve.

Influence of mass ratio on performance of 3D-Ti/PbO_2/AC AEC

In consideration of the difference between 3D-Ti/PbO_2/AC AEC and ideal capacitor, the energy of 3D-Ti/PbO_2/AC AEC was not calculated from the equation for ideal capacitors (Eq. (5)) [12]:

$$E = (1/2)C(V_2^2 - V_1^2) \quad (5)$$

In our experiments, the definition formula was used to calculate the gravimetric specific capacitance (C_S) (Eq. (6)). The gravimetric energy density (E_S) and average gravimetric power density (P_S) were integrated from discharge curves (Eqs. (7) and (8)).

$$C_S = \frac{I\Delta t}{m\Delta u} \quad (6)$$

$$E_S = \frac{I\int u dt}{m} \quad (7)$$

$$P_S = \frac{E_s}{\Delta t} \quad (8)$$

In Eqs. (7) and (8), I is the constant current in galvanostatic charge–discharge process; t is time; u represents instantaneous voltage on the two terminals of 3D-Ti/PbO_2/AC AEC; m is the total mass of positive active material and negative active material; Δu is the voltage change in capacitive voltage range and Δt is the time change. In this study, the mass ratio of negative active material to positive active material was taken into consideration aiming to find the optimal mass ratio with which the energy density is the highest.

The charge–discharge curves of 3D-Ti/PbO_2/AC AEC are illustrated as a function of mass ratio in Fig. 6. Six different mass ratios were tested in this experiment. On the whole, in charge process, the increasing speed of voltage declined with increasing the mass of AC, indicating the increase of negative capacity; in discharge process, with increasing the mass of AC, the voltage of the inflexion point between the second part and third part of discharge curve increased, which indicates that the potential at the end of discharge of AC reduces. Furthermore, the increasing amount of AC enhances the area between the discharge curve and time coordinate, which is a signal that more energy is stored.

With a low mass ratio, the third part of the discharge curve did not decline fast, because the amount of AC is so little that its discharge time is too short. When the AC electrode discharged completely, oxygen evolution reaction occurred on the AC electrodes (Eq. (9)) and the potential retained at a relatively steady potential of about 1.0 V.

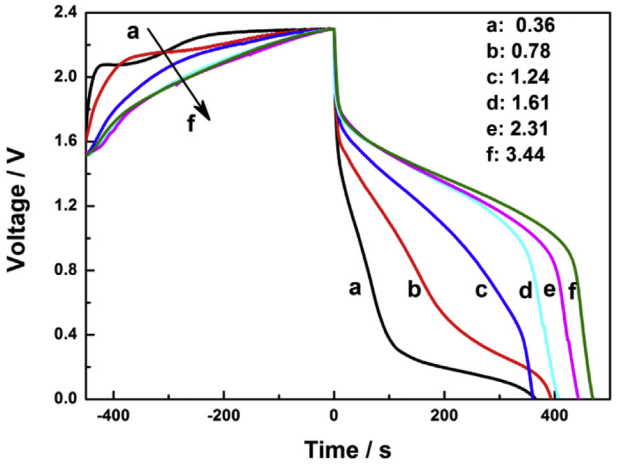

Fig. 6 – Charge–discharge curves of 3D-Ti/PbO_2/AC AEC as a function of mass ratio in 1.0 mol L^{-1} H_2SO_4 solution at current density of 10 mA cm^{-2}; The numbers in the figure are the mass ratio of negative active material to positive active material.

$$2H_2O \rightarrow O_2 + 4e^- + 4H^+ \quad (9)$$

Meanwhile, the discharge plateau of 3D-Ti/PbO_2 was about 1.3 V, so the voltage of inflexion point was about 0.3 V (plot a in Fig. 6). With further increasing the mass of AC, the voltage of inflexion point increased, which means that the whole capacitive potential range of −0.5 to 0.9 V of AC is not completely utilized. When the inflexion point went up to 0.8 V, the 3D-Ti/PbO_2/AC AEC obtained the highest energy density (Fig. 7). In the meantime, the potential at the end of discharge of AC was about 0.5 V, and the working potential range of AC was about −0.5 to 0.5 V. When the highest energy density was obtained, the mass ratio of negative active material to positive active material was 1.61. In consideration of the above discussion, the mass ratio is of great importance. If the mass of AC is too small, the oxygen evolution reaction will occur on AC

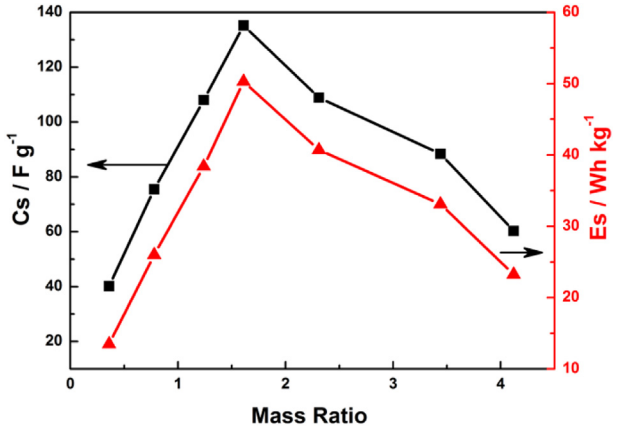

Fig. 7 – Influence of mass ratio on the specific capacitance and energy density; Results are integrated from the second part of discharge curves of 3D-Ti/PbO_2/AC AEC at discharge current density of 10 mA cm^{-2}.

and the AC electrode will experience oxidation [40], leading to a shortened lifespan. If the mass of AC is too large the energy density will be low.

The influence of mass ratio on specific capacitance and energy density is shown in Fig. 7. As shown in Fig. 7, specific capacitance and energy density increased initially with increasing mass ratio and then decreased when mass ratio surpassed 1.61. The specific capacitance and energy density were the highest when mass ratio was 1.61 with a specific capacitance of 135.2 F g^{-1} and an energy density of 49.4 Wh kg^{-1}. Within the above mentioned discussion, the PbO_2/AC AEC based on 3D-Ti/PbO_2 positive electrode has good capacitive behavior in the voltage range of 0.8–1.8 V with a mass ratio of 1.61. Besides, the side reactions such as oxidation of AC and oxygen evolution can be avoided. The voltage of inflexion point at 0.8 V can be a symbol of good matching for obtaining the highest energy density in PbO_2/AC AEC, as described in literature [12].

Influence of current density on performance of 3D-Ti/PbO_2/AC AEC

Fig. 8 shows the discharge curves of 3D-Ti/PbO_2/AC AEC at different current densities. When the AEC discharged at a current density of 10 mA cm^{-2}, the discharge time was about 370 s. The discharge depth of positive electrode was about 72% indicating the incomplete discharge of 3D-Ti/PbO_2, which could lead to a long lifespan of 3D-Ti/PbO_2/AC AEC. The capacity of 3D-Ti/PbO_2/AC AEC declined with increasing the discharge current density. This mainly results from 3D-Ti/PbO_2, because the capacity of AC electrode declines much slower than that of 3D-Ti/PbO_2 [41].

Fig. 9 shows the dependence of energy density and specific capacitance change upon charge–discharge current densities. On the whole, both energy density and specific capacitance declined with increasing charge–discharge current density. The insert is Ragone plot which shows the dependence of energy density upon average power density. When the 3D-Ti/PbO_2/AC AEC delivered a power density of 433.2 W kg^{-1}, the energy density was 49.4 Wh kg^{-1}. When the 3D-Ti/PbO_2/AC AEC delivered a power density as high as 2078 W kg^{-1}, the energy density still retained at 30 Wh kg^{-1} indicating the good power performance of 3D-Ti/PbO_2/AC AEC.

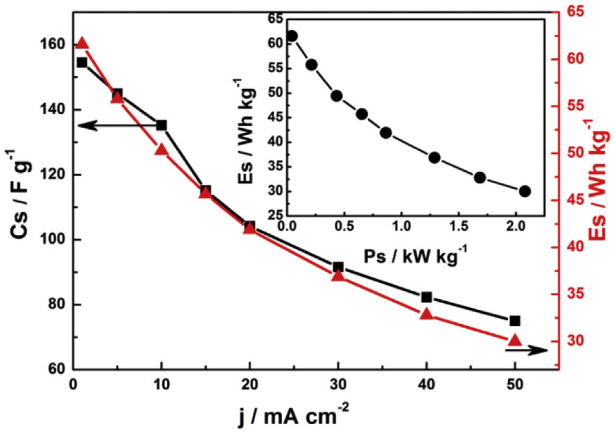

Fig. 9 – Influence of charge–discharge current density on the specific capacitance and energy density of 3D-Ti/PbO_2/AC AEC; Results are integrated from the voltage range of 0.8–1.8 V of discharge curves; The insert is Ragone plot.

Impedance and cycling performances of 3D-Ti/PbO_2/AC AEC

In order to understand the interfacial process of 3D-Ti/PbO_2/AC AEC, EIS was applied in this study. The EIS data is presented in Fig. 10 in the form of Nyquist plot. The Nyquist plot comprised two sections: the semicircle at high frequency range followed by the oblique line at low frequency range. It is an indication that the electrochemical reaction was controlled by charge transfer at high frequency range and was controlled by electrolyte diffusion at low frequency range. To obtain the interfacial details of 3D-Ti/PbO_2/AC AEC, a phenomenological equivalent circuit (insert in Fig. 10) was applied in the simulation of the EIS data. In the equivalent circuit, R_s represents the ohmic resistance of AEC including electrolyte resistance,

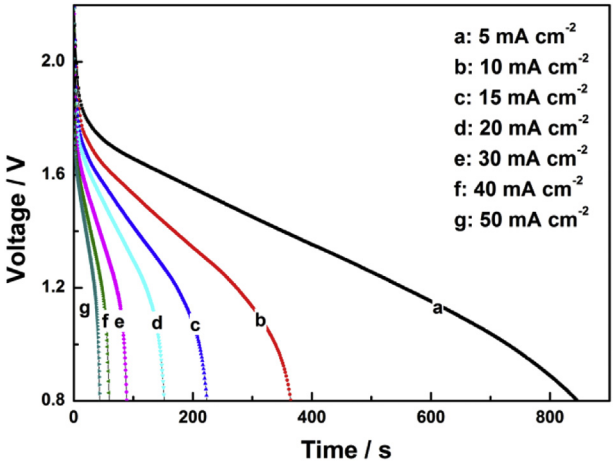

Fig. 8 – Discharge curves of 3D-Ti/PbO_2/AC AEC as a function of current density in 1.0 mol L^{-1} H_2SO_4 with the cut off voltage of 0.8 V.

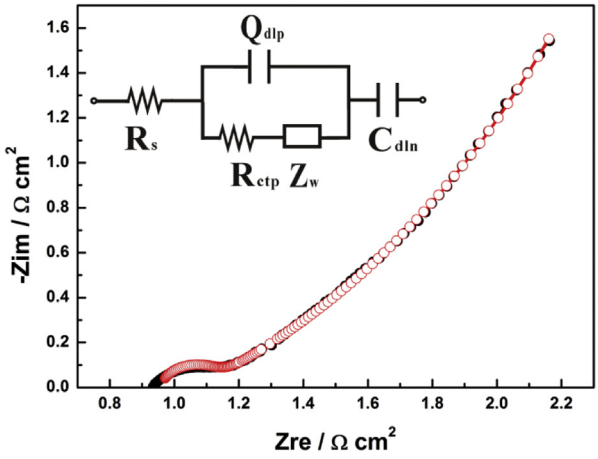

Fig. 10 – Nyquist plot of 3D-Ti/PbO_2/AC AEC measured at 1.8 V; Solid circle (●) and empty circle (○) represent the measured data and the simulated data, respectively; The insert is the equivalent circuit.

Table 1 – Simulated values of each electrical element in the equivalent electrical circuit.

Element	R_s	Q_{dlp}	n	R_{ctp}	Z_w	C_{dln}	χ^2
	$\Omega\ cm^2$	$\Omega^{-1}\ cm^{-2}\ s^n$	–	$\Omega\ cm^2$	$\Omega\ cm^2$	$F\ cm^{-2}$	–
Value	0.9598	5.388×10^{-4}	0.9572	0.1842	0.2595	0.32557	1.47×10^{-4}

external resistance, contact resistance, resistance of active materials and so forth. The constant phase element (CPE) Q_{dlp} represents the non-ideal electrical double layer behavior of the PbO_2/H_2SO_4 interface. R_{ctp} represents the charge transfer resistance of positive electrode. Z_w represents the Warburg impedance. C_{dln} is the capacitance of AC negative electrode.

The equivalent series resistance (ESR) of 3D-Ti/PbO_2/AC AEC was determined as the real impedance at 1 kHz. The ESR of AEC was about 1.11 $\Omega\ cm^2$. These two values are much smaller than the data in literature [12], which is attributed to large electrochemical active surface area of 3D-Ti/PbO_2. The simulated results are listed in Table 1. The small value of χ^2 indicates a good simulation. The ESR is equivalent to the summation of R_s and R_{ctp}, and the ESR determined from Nyquist plot is equal to the summation of R_s and R_{ctp} approximately. The similarity between measured results and simulated results indicate the good representativeness of equivalent circuit of 3D-Ti/PbO_2/AC AEC.

Fig. 11 shows the galvanostatic cycling stability of 3D-Ti/PbO_2/AC AEC. The end voltage of charge and cut off voltage of discharge were controlled at 2.3 and 0.8 V, respectively. The capacitance increased at the initial cycles due to the transformation from α-PbO_2 to β-PbO_2, and reached the highest value after about 200 cycles. The capacitance of 3D-Ti/PbO_2/AC AEC retained 99.2% after 1000 cycles with coulombic efficiencies of about 93% within one thousand cycles.

Conclusions

3D-Ti/PbO_2 with high specific capacity was electrodeposited on 3D porous titanium. A PbO_2/AC asymmetric electrochemical capacitor (AEC) was further fabricated based on the 3D-Ti/PbO_2 positive electrode with corresponding AC as negative electrode. The PbO_2/AC AEC obtained the highest energy density of 49.4 Wh kg^{-1} (corresponding specific capacitance 135.2 F g^{-1}) with mass ratio of 1.61 at charge–discharge current density of 0.9 A g^{-1}, with the corresponding power density of 433.2 W kg^{-1}. The energy density of 3D-Ti/PbO_2/AC AEC has been improved greatly compared with the highest value in literature and is even comparable to that of lead acid batteries. The high energy density of 3D-Ti/PbO_2/AC AEC resulted from the high specific capacity of 3D-Ti/PbO_2. In summary, the PbO_2/AC AEC based on 3D-Ti/PbO_2 has high energy density over traditional electrochemical capacitors and long lifespan over traditional lead acid batteries. It is a promising energy storage device which could be used in long-term energy storage applications such as load leveling and renewable energy storage.

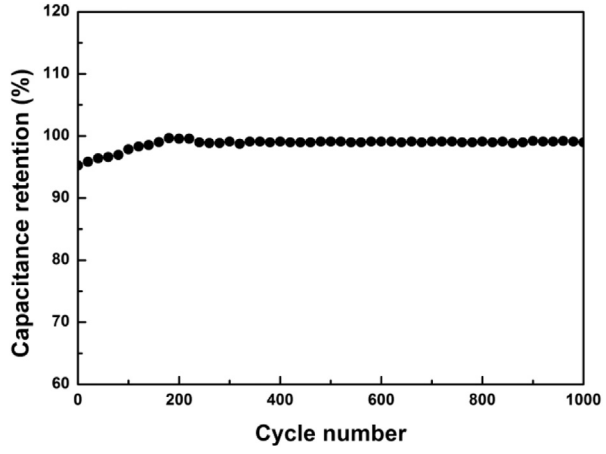

Fig. 11 – Galvanostatic cycling stability of 3D-Ti/PbO_2/AC AEC at current of 5 mA cm^{-2}, when the end voltage of charge is 2.3 V and the cut off voltage of discharge is 0.8 V.

Acknowledgments

The research group acknowledges the financial support provided by the National Natural Science Foundation of China (No. 21273097) and the Key Project in Jilin Province (No. 20126010).

REFERENCES

[1] Armaroli N, Balzani V. Towards an electricity-powered world. Energy Environ Sci 2011;4:3193–222.
[2] González I, Ramiro A, Calderón M, Calderón AJ, González JF. Estimation of the state-of-charge of gel lead-acid batteries and application to the control of a stand-alone wind–solar test-bed with hydrogen support. Int J Hydrogen Energy 2012;37:11090–103.
[3] Lemaire-Potteau E, Vallve X, Pavlov D, Papazov G, Van der Borg N, Sarrau JF. ABLE project: development of an advanced lead-acid storage system for autonomous PV installations. J Power Sources 2006;162:884–92.
[4] Wagner R. Large lead/acid batteries for frequency regulation, load leveling and solar power applications. J Power Sources 1997;67:163–72.
[5] Perrin M, Saint-Drenan YM, Mattera F, Malbranche P. Lead-acid batteries in stationary applications: competitors and new markets for large penetration of renewable energies. J Power Sources 2005;144:402–10.
[6] Bullock KR. Lead acid battery systems and technology for sustainable energy. In: Meyers RA, editor. Encyclopedia of sustainability science and technology. New York: Springer; 2012. p. 117–34.
[7] Lam LT, Haigh NP, Phyland CG, Urban AJ. Failure mode of valve-regulated lead-acid batteries under high-rate partial-state-of-charge operation. J Power Sources 2004;133:126–34.
[8] Huang KJ, Wang L, Liu YJ, Liu YM, Wang HB, Gan T, et al. Layered MoS_2-graphene composites for supercapacitor

applications with enhanced capacitive performance. Int J Hydrogen Energy 2013;38:14027–34.
[9] Zhang YK, Li JL, Kang FY, Gao F, Wang XD. Fabrication and electrochemical characterization of two-dimensional ordered nanoporous manganese oxide for supercapacitor applications. Int J Hydrogen Energy 2012;37:860–9.
[10] Zhang Y, Feng H, Wu X, Wang L, Zhang A, Xia T, et al. Progress of electrochemical capacitor electrode materials: a review. Int J Hydrogen Energy 2009;34:4889–99.
[11] Shukla AK, Banerjee A, Ravikumar MK, Jalajakshi A. Electrochemical capacitors: technical challenges and prognosis for future markets. Electrochim Acta 2012;84:165–73.
[12] Yu N, Gao L, Zhao S, Wang Z. Electrodeposited PbO_2 thin film as positive electrode in PbO_2/AC hybrid capacitor. Electrochim Acta 2009;54:3835–41.
[13] Yu N, Gao L. Electrodeposited PbO_2 thin film on Ti electrode for application in hybrid supercapacitor. Electrochem Commun 2009;11:220–2.
[14] Pavlov D. Lead-acid batteries: science and technology. Amsterdam: Elsevier; 2011.
[15] Ruetschi P. Aging mechanisms and service life of lead-acid batteries. J Power Sources 2004;127:33–44.
[16] Yan JH, Li WS, Zhan QY. Failure mechanism of valve-regulated lead-acid batteries under high-power cycling. J Power Sources 2004;133:135–40.
[17] Zhou D, Gao L. Effect of electrochemical preparation methods on structure and properties of PbO_2 anodic layer. Electrochim Acta 2007;53:2060–4.
[18] Velichenko AB, Amadelli R, Gruzdeva EV, Luk'yanenko TV, Danilov FI. Electrodeposition of lead dioxide from methanesulfonate solutions. J Power Sources 2009;191:103–10.
[19] Ghasemi S, Mousavi MF, Karami H, Shamsipur M, Kazemi SH. Energy storage capacity investigation of pulsed current formed nano-structured lead dioxide. Electrochim Acta 2006;52:1596–602.
[20] Chen T, Huang H, Ma H, Kong D. Effects of surface morphology of nanostructured PbO_2 thin films on their electrochemical properties. Electrochim Acta 2013;88:79–85.
[21] Egan DRP, Low CTJ, Walsh FC. Electrodeposited nanostructured lead dioxide as a thin film electrode for a lightweight lead-acid battery. J Power Sources 2011;196:5725–30.
[22] Vatistas N, Cristofaro S. Lead dioxide coating obtained by pulsed current technique. Electrochem Commun 2000;2:334–7.
[23] Shen PK, Wei XL. Morphologic study of electrochemically formed lead dioxide. Electrochim Acta 2003;48:1743–7.
[24] Ghasemi S, Karami H, Mousavi MF, Shamsipur M. Synthesis and morphological investigation of pulsed current formed nano-structured lead dioxide. Electrochem Commun 2005;7:1257–64.
[25] Perret P, Brouss T, Bélanger D, Guay D. Electrochemical template synthesis of ordered lead dioxide nanowires. J Electrochem Soc 2009;156:A645–51.
[26] Bartlett PN, Dunford T, Ghanem MA. Templated electrochemical deposition of nanostructured macroporous PbO_2. J Mater Chem 2002;12:3130–5.
[27] Perret P, Khani Z, Brousse T, Bélanger D, Guay D. Carbon/PbO_2 asymmetric electrochemical capacitor based on methanesulfonic acid electrolyte. Electrochim Acta 2011;56:8122–8.
[28] Chen Y, Chen BZ, Ma LW, Yuan Y. Effect of carbon foams as negative current collectors on partial-state-of-charge performance of lead acid batteries. Electrochem Commun 2008;10:1064–6.
[29] Jang YI, Dudney NJ, Tiegs TN, Klett JW. Evaluation of the electrochemical stability of graphite foams as current collectors for lead acid batteries. J Power Sources 2006;161:1392–9.
[30] Sun J, Lu H, Lin H, Huang W, Li H, Lu J, et al. Boron doped diamond electrodes based on porous Ti substrates. Mater Lett 2012;83:112–4.
[31] Kong H, Lu H, Zhang W, Lin H, Huang W. Performance characterization of Ti substrate lead dioxide electrode with different solid solution interlayers. J Mater Sci 2012;47:6709–15.
[32] Sáez V, Marchante E, Díez MI, Esclapez MD, Bonete P, Lana-Villarreal T, et al. A study of the lead dioxide electrocrystallization mechanism on glassy carbon electrodes. Part I: experimental conditions for kinetic control. Mater Chem Phys 2011;125:46–54.
[33] Sirés I, Low CTJ, Ponce-de-León C, Walsh FC. The characterisation of PbO_2-coated electrodes prepared from aqueous methanesulfonic acid under controlled deposition conditions. Electrochim Acta 2010;55:2163–72.
[34] Vogt H. Note on a method to interrelate inner and outer electrode areas. Electrochim Acta 1994;39:1981–3.
[35] Takasu Y, Murakami Y. Design of oxide electrodes with large surface area. Electrochim Acta 2000;45:4135–41.
[36] Ardizzone S, Fregonara G, Trasatti S. "Inner" and "outer" active surface of RuO_2 electrodes. Electrochim Acta 1990;35:263–7.
[37] Montilla F, Morallón E, De Battisti A, Vázquez JL. Preparation and characterization of antimony-doped tin dioxide electrodes. Part 1. Electrochemical characterization. J Phys Chem B 2004;108:5036–43.
[38] Carr JP, Hampson NA. Lead dioxide electrode. Chem Rev 1972;72:679–703.
[39] Pavlov D, Kirchev A, Stoycheva M, Monahov B. Influence of H_2SO_4 concentration on the mechanism of the processes and on the electrochemical activity of the Pb/PbO_2/$PbSO_4$ electrode. J Power Sources 2004;137:288–308.
[40] Babeł K, Jurewicz K. KOH activated lignin based nanostructured carbon exhibiting high hydrogen electrosorption. Carbon 2008;46:1948–56.
[41] Li J, Gao F. Analysis of electrodes matching for asymmetric electrochemical capacitor. J Power Sources 2009;194:1184–93.